Full Paper

Israel Journal of Chemistry

DOI: 10.1002/ijch.201600076

Formation of Apoptosis-Inducing Amyloid Fibrils by Tryptophan

Shira Shaham-Niv,[a] Pavel Rehak,[b] Lela Vuković,[c] Lihi Adler-Abramovich,[d] Petr Král,[b, e, f] and Ehud Gazit*[a, g]

Abstract: Many major degenerative disorders are associated with the formation of amyloid fibrils by proteins and peptides. Recent studies have extended the repertoire of amyloidogenic building blocks to non-proteinaceous entities, including amino acids and nucleobases. Here, based on the high propensity of tryptophan-containing proteins and peptides to form amyloid fibrils, we explored the self-assembly profile of this amino acid. We discovered that tryptophan forms fibrillary assemblies with a diameter of 15–75 nm. These fibrils bind the thioflavin T amyloid-specific dye and show a typical spectrum of amyloid proteins upon binding. Furthermore, the assemblies show significant cytotoxicity triggered by an apoptosis mechanism, similar to that known for amyloids. As a control, the non-amyloidogenic amino acid alanine was used under the same conditions and did not show any toxicity. Molecular dynamics simulations were used to explore the possible growth mechanism, molecular organization, and stability of tryptophan amyloidal fibrils. Taken together, we provide further extension to the amyloid hypothesis and additional indication for a knwon mechanism of toxicity for both amyloid-associated and metabolic disorders.

Keywords: aggregation · amino acids · amyloids · cytotoxicity · metabolic disorders

1. Introduction

Over the past decade, the phenomenon of soluble protein and peptide misfolding, leading to the formation of ordered amyloid fibrils, has been increasingly associated with a great variety of notable human disorders with unrelated etiology, including Alzheimer's disease, Parkinson's disease, and type II diabetes.[1] All amyloid fibrils share a unique set of similar biophysical and structural properties, despite being formed by a diverse and structurally unrelated group of proteins and peptides. These fibrillar supramolecular assemblies have a diameter of 5–20 nm, are predominantly rich in β-sheet secondary structure, and specifically bind dyes, such as thioflavin T (ThT) and Congo red.[2] Interestingly, analysis of short functional fragments from unrelated amyloid-forming proteins and polypeptides identified a remarkable occurrence of aromatic residues.[3] The aromatic residues most likely have an important role in the amyloidogenic process and in the stabilization of amyloidal structures by

[a] S. Shaham-Niv, E. Gazit
Department of Molecular Microbiology and Biotechnology
George S. Wise Faculty of Life Sciences
Tel Aviv University
Tel Aviv 69978 (Israel)

[b] P. Rehak, P. Král
Department of Chemistry
University of Illinois at Chicago
Chicago (USA)

[c] L. Vuković
Department of Chemistry
University of Texas at El Paso
El Paso (USA)

[d] L. Adler-Abramovich
Department of Oral Biology
The Goldschleger School of Dental Medicine
Tel Aviv University
Tel Aviv 69978 (Israel)

[e] P. Král
Department of Physics
University of Illinois at Chicago
Chicago (USA)

[f] P. Král
Department of Biopharmaceutical Sciences
University of Illinois at Chicago
Chicago (USA)

[g] E. Gazit
Department of Materials Science and Engineering
Iby and Aladar Fleischman Faculty of Engineering
Tel Aviv University
Tel Aviv 69978 (Israel)
Tel.: (+972) 3-640-9030
e-mail: ehudg@post.tau.ac.il

Supporting information for this article is available on the WWW under http://dx.doi.org/10.1002/ijch.201600076.

© 2017 Wiley-VCH Verlag GmbH & Co. KGaA, Weinheim

geometrically restricted interactions between planar aromatic chemical entities. These residues can affect the morphology of the assemblies, accelerate their formation, improve their stability and reduce the minimal association concentration.[4] It was previously shown that penta- and tetrapeptides can form typical amyloid fibrils. Moreover, the diphenylalanine dipeptide, the core recognition motif within the β-amyloid polypeptide, was found to form well-ordered nanotubular assemblies in aqueous solution.[5] Later on, these dipeptide assemblies were shown to share optical and functional properties with amyloids that were assembled from the full-length polypeptide.[6] The pentapeptide- and tetrapeptide-based amyloid nanoassemblies were found to be cytotoxic via an apoptotic cell death pathway, which indicates a biological generic property and a common mechanism of toxicity.[7] Thus the minimal peptide assemblies appear to reflect both the physical as well as functional properties of natural amyloid fibrils.

While the formation of cytotoxic supramolecular entities has previously been linked to proteins and peptides, it was first demonstrated by our group and later by others that phenylalanine, as a single amino acid, can also self-assemble to form amyloid-like fibrils showing typical ultrastructural, biophysical, and biochemical properties.[8] Moreover, we revealed the connection between these assemblies and the accumulation of phenylalanine in phenylketonuria (PKU), a known metabolic disorder. We demonstrated that these phenylalanine assemblies are cytotoxic and that antibodies raised towards these species deplete fibril toxicity. The generation of antibodies in a PKU mice model and the identification of aggregate deposits in patients' brains post mortem suggested a pathological role of these assemblies.[8a]

Metabolic disorders, such as PKU, and more specifically inborn errors of metabolism, are the result of a flaw in a single gene encoding for metabolic enzymes. As a result, accumulating metabolites may interfere with the normal function of cells and tissues and thus cause severe abnormalities. Unless these inherited disorders are treated with a very strict diet, they may result in mental retardation and other developmental problems. Although these disorders are individually considered very rare, collectively they constitute a very substantial part of pediatric genetic diseases.[9] Recently, we have extended the generic amyloid hypothesis to include additional non-proteinaceous entities, including amino acids and nucleobases. We demonstrated the ability of these small metabolites to form amyloidal fibrils, sharing the same biophysical properties, as presented by electron microscopy and the ThT binding assay, and their clear apoptotic effect on a neuronal cell model. These new findings introduce a new possible amyloid-like mechanism of metabolic disorders, suggesting a new paradigm for these rare maladies.[10]

Previous work that examined the amyloid aggregation propensity of all 20 coded amino acids revealed that cysteine, phenylalanine, and tyrosine have high aggregation potential,[11] in agreement with their potential aggregative property as isolated amino acids.[10] However, the highest propensity was calculated for tryptophan,[11] which was not found in our initial screen. In addition, the high aggregation ability of tryptophan was also shown in the context of tripeptides, where the amino acid exhibited high aggregation propensity when positioned in the N-terminal, middle, or C-terminal positions.[12] The aromatic amino acid tryptophan (see Figure 1A) is essential for humans, playing a crucial role in protein stability and recognition, despite its rarity in protein sequences.[13] Furthermore, tryptophan is a critical component of numerous metabolic pathways, being a biochemical precursor for serotonin, melatonin, and niacin.[14] Tryptophan is accumulated in pathological conditions, such as several metabolic disorders. The accumulation of tryptophan has been reported in two inborn errors of metabolism, hypertryptophanemia and Hartnup disease (see Table 1), both shown to be rare and inherited autosomal recessive disorders. Hypertryptophanemia occurs due to the inability of the body to process tryptophan. As a result, there is a massive buildup of tryptophan in the blood and urine, which further leads to musculoskeletal effects and to behavioral and developmental abnormalities.[15] Hartnup disease is caused by damage to a neutral amino acid transporter, limited to the kidneys and small intestine, which affects the absorption of nonpolar amino acids, mainly tryptophan. Thus, increased levels of tryptophan and indolic compounds are detected in the patients' urine. Common symptoms include the development of a rash on parts of the body exposed to the sun, mental retardation, headaches, collapsing and fainting.[16]

In light of the above findings, we screened for conditions in which tryptophan could form visible structures and found that by increasing tryptophan concentration, using the same conditions for self-assembly as with other metabolites, we could detect the formation of assemblies in the test tube. The properties of these assemblies were further examined using lower concentrations, similar to the ones used in our previous screening. Here we present, for the first time, the ability of the single amino acid tryptophan to form amyloid supramolecular assemblies. We characterized the tryptophan aggregates using a combination of diverse biophysical and biological assays, in addition to the use of molecular dynamics (MD) simulations to model the fibril formation and stability. This work further extends the generic amyloid hypothesis and gives further supporting evidence for the association between metabolite amyloid formation and metabolic pathologies.

2. Experimental Results and Discussion

In previous work that calculated the amyloid aggregation potential of all amino acids in the context of proteins and

© 2017 Wiley-VCH Verlag GmbH & Co. KGaA, Weinheim

Israel Journal of Chemistry

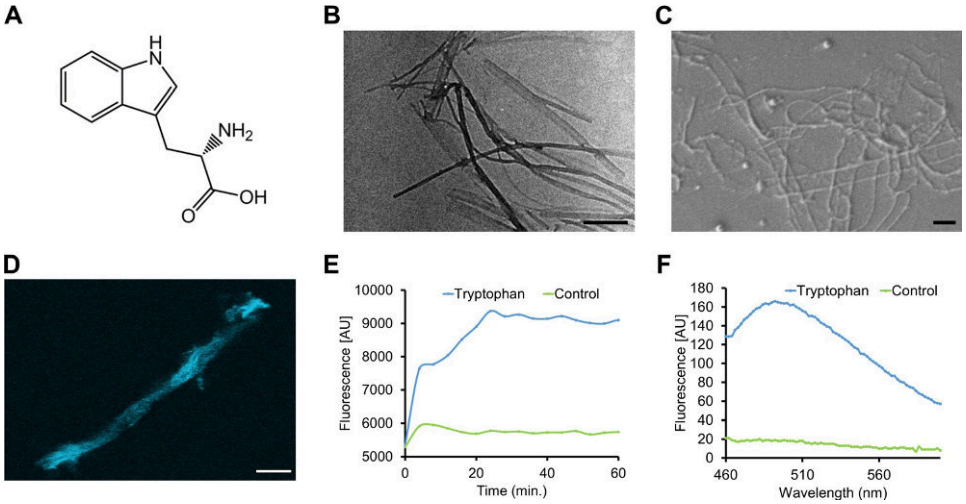


Figure 1. Formation of amyloid-like structures by tryptophan self-assembly. For all assays, tryptophan (4 mg/mL) was dissolved at 90 °C in PBS and cooled down gradually for the formation of structures. (A) Tryptophan skeletal formula. (B) TEM micrograph of tryptophan assemblies. Scale bar is 500 nm. (C) HR-SEM micrograph of tryptophan assemblies. Scale bar is 500 nm. (D) Confocal fluorescence microscopy image of tryptophan assemblies stained with ThT. Images were taken immediately after the addition of the ThT reagent (final concentration 20 μM ThT). Excitation and emission wavelengths were 458 and 485 nm, respectively. Scale bar is 20 μm. (E) ThT fluorescence assay of tryptophan assemblies. Tryptophan (4 mg/mL) was dissolved in PBS at 90 °C, followed by the addition of ThT to a final concentration of 20 μM. ThT emission data at 480 nm (excitation at 450 nm) was measured over time. (F) ThT fluorescence emission spectra of tryptophan assemblies (4 mg/mL) following excitation at 430 nm. Aged samples were added to 40 μM ThT in PBS to a final concentration of 20 μM ThT. The control reflects addition of PBS to 40 μM ThT in PBS to a final concentration of 20 μM ThT.

Table 1. Amino acids with high amyloid aggregation propensity and the genetic inborn error of metabolism disorders in which they accumulate (the order corresponds to their calculated amyloidogenic potential[11]).

Metabolite	Disorder
Tryptophan	Hypertryptophanemia, Hartnup disease
Phenylalanine	Phenylketonuria
Cystine	Cystinuria, Cystinosis
Tyrosine	Tyrosinemia
Isoleucine	Maple syrup urine disease
Valine	Isobutyryl-CoA dehydrogenase deficiency, Maple syrup urine disease

polypeptides, the amino acids tryptophan, phenylalanine, cysteine, tyrosine, isoleucine, and valine were found to have positive propensity to form amyloid assemblies.[11] These amino acids were also found to accumulate in genetic inborn error of metabolism disorders (Table 1).[17]

Initial screening performed by our group revealed that phenylalanine, cystine, and tyrosine can self-assemble to form elongated amyloid fibrils. In order to mimic physiological conditions, the amino acids were dissolved in phosphate-buffered saline (PBS), which reflects physiological pH and ionic strength. To obtain a homogenous monomeric solution, the amino acids were dissolved at 90 °C in physiological buffer, followed by gradual cooling of the solution.[10] Here, we maintained the same conditions in terms of buffer composition and temperature; however, higher concentrations of tryptophan, compared to those used for the initial screen, were tested. Interestingly, at a high concentration of 40 mg/mL in PBS, which was heated to 90 °C and allowed to gradually cool, structures were formed in the tested samples. For further examinations, we decreased the tryptophan concentration and used the same concentrations we used for the self-assembly of the other aromatic amino acids, phenylalanine and tyrosine.

Next, we characterized the structure of tryptophan assemblies and examined whether they possess the hallmarks of ordered amyloid structures. As discussed above, amyloid fibrils share a set of biophysical properties, showing the morphology of elongated fibrils with a typical diameter of 5–20 nm. In addition, they self-assemble to form ordered β-sheet secondary structures, which can be detected using the typical amyloid dye ThT. This amyloid-specific reagent changes its fluorescence upon interaction with ordered amyloid assemblies, which can be further monitored using fluorescence microscopy, measurements of ThT emission data at 480 nm (excitation at 450 nm) over time, and measurements of fluorescence emission spectra. Indeed, using transmission electron microscopy (TEM) and high-resolution scanning electron microscopy (HR-SEM), the tryptophan assemblies were found to present an elongated fibrillar morphology, similar to that observed for common amyloid aggregates, with a diameter of 15–75 nm (see Figure 1B, C). Furthermore, a typical change in the ThT fluorescence signal was detected in the presence of these fibrils, as shown using con-

 © 2017 Wiley-VCH Verlag GmbH & Co. KGaA, Weinheim

focal fluorescence microscopy, where a bundle of fluorescent fibrils was observed (see Figure 1D). In addition, these fibrils presented a distinctive time-dependent fluorescence curve and emission fluorescence spectra correlating to those of amyloid assemblies (see Figure 1E, F).

As mentioned above, amyloid aggregates not only share common ultrastructural and biophysical properties but also resemble amyloids in their ability to cause cytotoxicity. As mentioned, an increasing amount of major human neurodegenerative diseases are associated with misfolding of proteins and peptides, resulting in the formation of amyloid fibrils, which are likely to be the central factor in the pathology of these diseases. These fibrillary deposits are located in the intracellular or extracellular matrix, where they can disrupt the normal function of cells and organs, leading to notable cell death.[1e,7a,18] Therefore, the ability of the tryptophan amyloid assemblies to cause cytotoxicity was examined. A set of increasing tryptophan concentrations (0.2, 2 and 4 mg/mL) were tested, corresponding to the set of concentrations used in our previous work with other metabolites.[10] These tryptophan assemblies were added to the SH-SY5Y cell line, which is often used as an in vitro model of neuronal function. To assure formation of tryptophan fibrils, tryptophan was dissolved at 90 °C in cell medium followed by gradual cooling of the solution, allowing the formation of assemblies overnight. As observed using a 2,3-bis(2-methoxy-4-nitro-5-sulfophenyl)-2*H*-tetrazolium-5-carboxanilide (XTT) cell viability assay, tryptophan assemblies presented a clear dose-dependent effect on cell viability, decreasing the percentage of live cells to 23 % and 40 % at 4 mg/mL and 2 mg/mL, respectively (Figure 2A). Alanine, an amino acid that does not accumulate in any metabolic disorder, has low propensity to aggregate,[11] and does not self-assemble under these conditions, was used as a control, demonstrating that the effect on cell viability was due to the tryptophan assemblies and was not caused by the high concentration of the amino acid. The alanine control demonstrated no significant effect on cell viability, even at the high concentration of 4 mg/mL (see Figure 2B).

Amyloid proteins and peptides have been reported to trigger degeneration of cultured neuron cells through activation of an apoptotic pathway. Apoptosis, in contrast to necrosis, is a type of well-regulated cell death, occurring asynchronously in cell population, consistent with the progression of neurodegenerative diseases, and thus is considered to play a role in these maladies.[7b] In light of the suggested mechanism, the ability of tryptophan amyloid fibrils to cause not only cell death, but more specifically to trigger apoptotic cell death, was explored. For this purpose, an annexin V propidium iodide (PI) apoptosis assay was performed using the same tryptophan concentrations as in the XTT cell viability assay. The results clearly demonstrated that both late and early apoptosis are the main pathways causing SH-SY5Y cell death following treatment with tryptophan assemblies (Figure 3). Lower percentages of live cells were observed using this assay, reaching only 17 % and 20 % of live cells at 4 mg/mL and 2 mg/mL, respectively, due to a longer incubation period of the tryptophan structures with the neuronal cell model. As before, the alanine negative control did not demonstrate any apoptotic response on the examined cells (see Figure S1 in the Supporting Information).

3. Molecular Dynamics Simulations

To examine the possible structures of fibrils formed by tryptophan in its assembly process and the potential way in which tryptophan assemblies could exhibit a stable unidirectional growth, atomistic molecular dynamics (MD) simulations were used.[19] Figure 4 shows different tryptophan crystal assemblies that were simulated. In the simu-

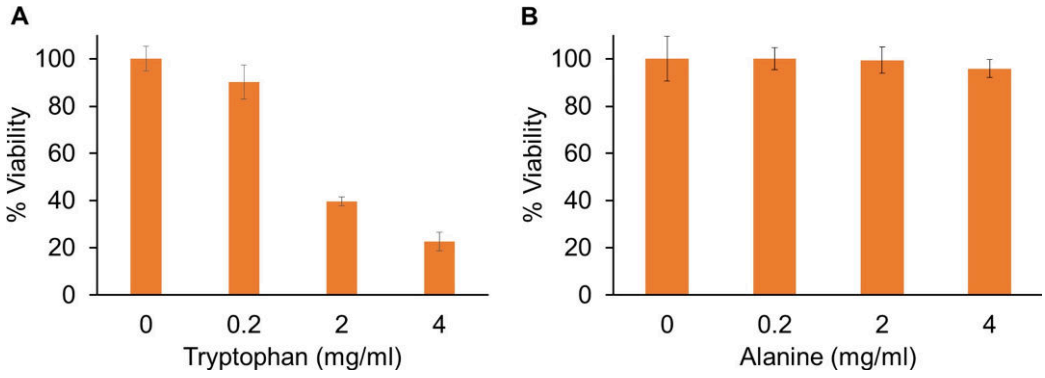


Figure 2. Cytotoxicity of the tryptophan assemblies as determined by XTT cell viability assay. (A) Tryptophan or (B) alanine were dissolved in cell medium at 90 °C followed by gradual cooling of the solution, allowing the formation of assemblies overnight. The control, namely zero concentration of tryptophan or alanine, reflects medium with no amino acids, which was treated in the same manner. The next day, SH-SY5Y cells were incubated with medium containing tryptophan assemblies or alanine at the stated concentrations for six hours, followed by the addition of the XTT reagent. After 2.5 hours of incubation, absorbance was determined at 450 nm. The results represent three independent biological repetitions.

© 2017 Wiley-VCH Verlag GmbH & Co. KGaA, Weinheim

Israel Journal of Chemistry

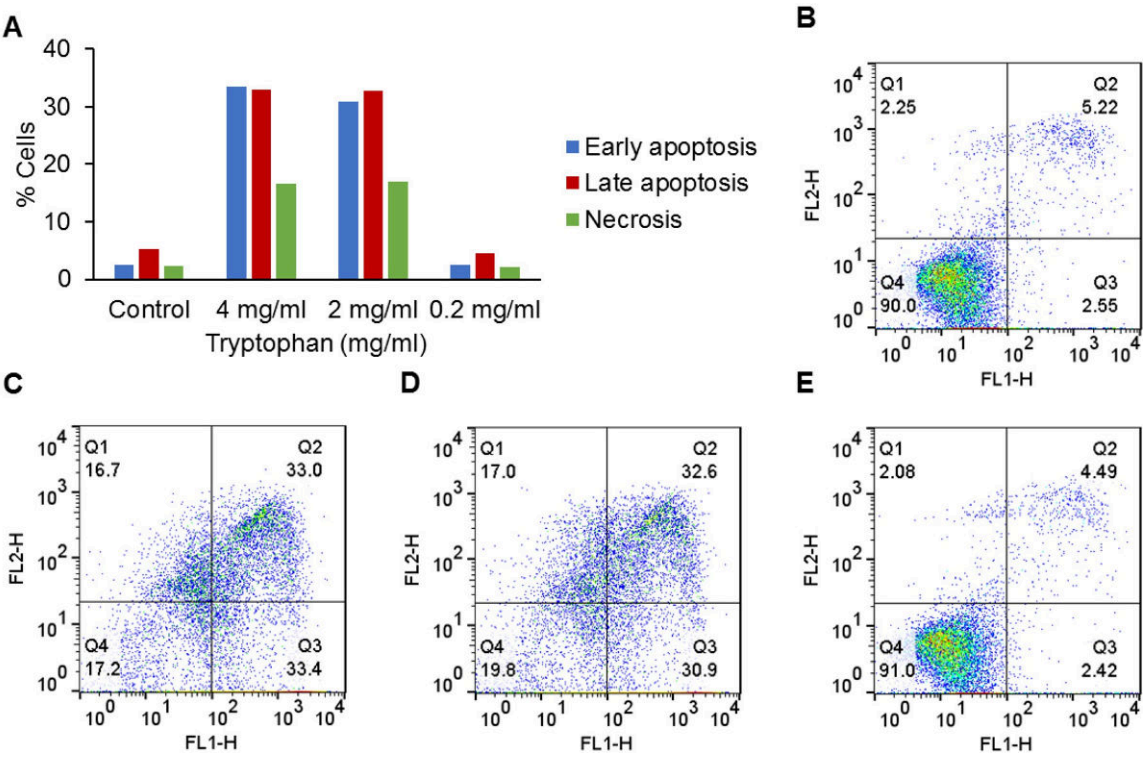


Figure 3. Apoptotic activity of the tryptophan assemblies studied by annexin V and PI assay. Tryptophan was dissolved at 90 °C in cell medium followed by gradual cooling of the solution. The control reflects medium that was treated in the same manner. SH-SY5Y cells were incubated with medium containing tryptophan at the stated concentrations for 24 hours. Control cells were incubated with medium without any addition of tryptophan. After incubation, annexin V–FITC and PI reagents were added to the cell cultures followed by measurement of the cell samples by flow cytometry using a single laser emitting excitation light at 488 nm. (A) Chart presenting calculated analysis of flow cytometry results. Analyses were performed using the FlowJo software (TreeStar, Version 14). Early apoptosis is represented in blue, late apoptosis in red, and necrosis in green. The results represent three independent biological repetitions. (B–E) Plots representing the annexin V/PI double-staining assays of cells incubated with or without tryptophan assemblies. Q1, PI(+) (cells undergoing necrosis); Q2, annexin V–FITC(+) PI(+) (cells in the late period of apoptosis and undergoing secondary necrosis); Q3, annexin V–FITC(−) PI(−) (live cells); Q4, annexin V–FITC(+) PI(−) (cells in the early period of apoptosis). (B) Control. (C) Tryptophan 4 mg/mL. (D) Tryptophan 2 mg/mL. (E) Tryptophan 0.2 mg/mL.

lations, we assumed that the molecular structure of the fibril is essentially based on the molecular structure of the bulk crystal,[19] in analogy to phenylalanine and diphenylalanine assemblies, which have related molecular structures in fibril and bulk crystal assemblies.[23,24] However, the bulk structure in the experimentally observed linear fibrils might have some degree of folding or reorganization that allows it to maintain one dominant growth direction. For example, in many materials whose bulk structures are formed by relatively weakly bound stacked layers (e.g., graphene organization of carbon), the individual layers can form kinetically stable nanotubes under suitable conditions. In a similar way, bulk tryptophan crystallizes in the form of bilayers, where the polar and nonpolar groups stay separated, and the polar zwitterionic groups stabilize the bilayers by hydrogen bonds and coulombic interactions between zwitterion groups. Such tryptophan bilayers can undergo some sort of folding into nanotubes or related structures.

To examine this possibility in our MD simulations, we simulated a small tryptophan bilayer formed by 288 tryptophan molecules organized in a membrane-like structure with middle zwitterion groups bound by hydrogen bonds (Figure 4A, B), a small triple tryptophan bilayer formed by 1536 tryptophan molecules (Figure 4C, D), and three differently cut tryptophan bilayers formed by 640, 640, and 3200 tryptophan molecules (Figure 4F–H). The structures of tryptophan crystals were simulated in 0.15 M NaCl solution (corresponding to the ionic strength of the physiological solution; more details are reported in the Experimental Section).

Figure 4A–D presents the two smaller systems at initial times and after 100–200 ns long simulations (see supplementary videos 1 and 2 in the Supporting Information). The monolayer has great flexibility, with the crystal bending in and out of the plane, whereas the trilayer is significantly more rigid. In both cases, only molecules from the edges and corners are seen to leave the crystals, while the

 © 2017 Wiley-VCH Verlag GmbH & Co. KGaA, Weinheim

Israel Journal of Chemistry

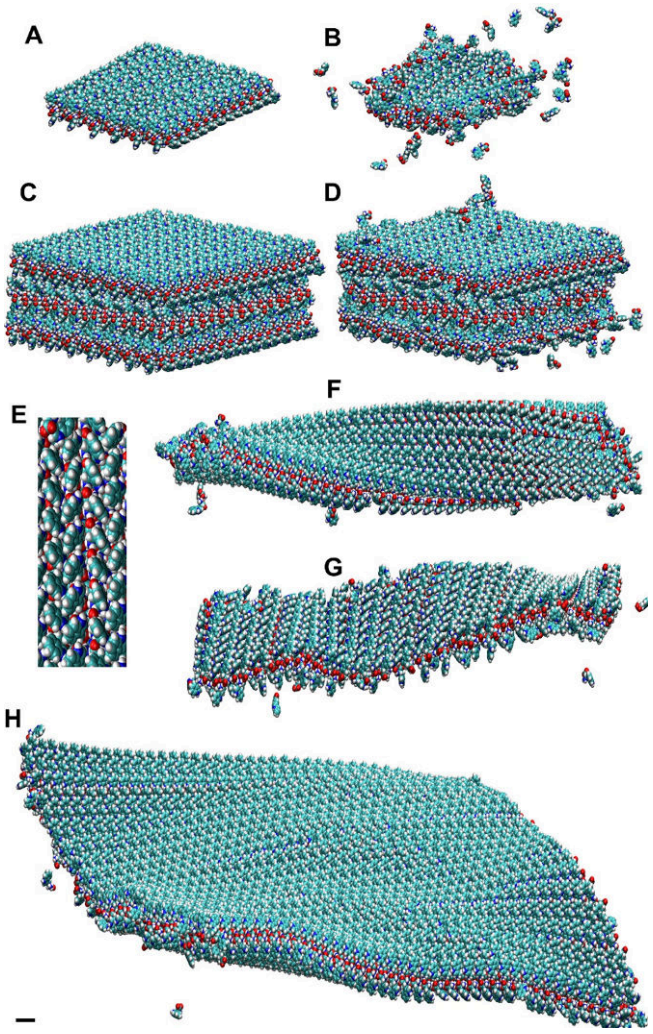


Figure 4. Modeling of hydrated tryptophan fibrils. (A,B) A tryptophan bilayer at times $t=0$, 244 ns. (C,D) A triple tryptophan bilayer at times $t=0$, 104 ns. All scale bars represent 10 Å. The bilayer bending fluctuates significantly over time, in contrast to the triple bilayer. The fluctuating bilayer also tends to release more molecules, but both systems remain mostly stable over time. (E) Detail of a tryptophan layer with exposed aromatic rings forming parallel 1D chains of paired rings. (F) An elongated tryptophan bilayer at the end of a 15 ns simulation. (G) Other tryptophan bilayers, cut along the orthogonal to parallel 1D chains of paired rings, after 12 ns, and (H) cut along both directions with respect to 1D chains of paired rings, after 6 ns.

top and bottom parts of the layers and the bulk of the crystals remained intact throughout the simulations. With a larger surface to volume ratio, the monolayer released a considerable number of molecules, showing the stabilization trend of larger crystal nuclei. This can be partly due to increased bending of the monolayer, destabilizing the molecules at its surface (edges). The amphiphilic tryptophan molecules that leave the crystals may recombine with molecules at the crystal sides via zwitterion–zwitterion attraction (edges become rounded). Even though zwitterions are strongly attracted to the aqueous environment, their coupling to other zwitterions in the crystals is preferential, since it is supported and protected by a mutual coupling of apolar aromatic head groups within the crystals. At times, free molecules are also observed to adsorb at the crystal (apolar) surfaces, but they do not form further layers under the conditions of the simulations performed (observation time, number of free molecules in the simulation box). These simulations support the idea that the crystals grow in the direction of bilayers, which might be twisted or folded to protect their edges. To understand better the preference towards 1D growth, we present in Figure 4E a detailed structure of a tryptophan layer with exposed aromatic rings forming parallel 1D chains of paired rings (six such parallel chains can be recognized in Figure 4A). Figure 4B shows that the chains of paired rings remain relatively rigid and stable during the simulations, while most of the layer bending proceeds in the direction orthogonal to these chains.

To further examine the hypothesis that the tryptophan layers may have a preference towards 1D growth, we simulated bilayers elongated in two separate directions (Figure 4F, G) and in both directions simultaneously (Figure 4H). All the bilayer structures fluctuate and bend. However, the fluctuations are mostly in the direction orthogonal to the chains of paired rings. Therefore, the structure that is cut along the chains (Figure 4F) is nicely twisted, while the orthogonally cut structure randomly fluctuates (Figure 4G). The large structure is twisted along the chains in an ambivalent manner at the two sides. These simulations demonstrate more clearly the possibility of tryptophan bilayer edges coming together to form a tubular structure in which chains of rings run parallel to the tube axis (Figure 4F). This tube could form the nucleus of a larger fibril, with the addition of new molecules occurring only at the tube edges along a single dimension or forming thicker multiwall tubular structures.

4. Conclusions

To conclude, in the current study we have presented the ability of the single tryptophan amino acid to self-associate into ordered supramolecular amyloid-like fibrils. Although many previous reports predicted the important role of tryptophan in the amyloid aggregation process, this is the first time where the amino acid alone is described to self-assemble into amyloid ultrastructures. The biophysical properties of the tryptophan assemblies were characterized using different methods, including both transmission and scanning electron microscopy, as well as the use of amyloid-specific dyes. Molecular dynamics simulations were used to examine a potential molecular organization of the tryptophan fibrils and their growth and stability. The simulations reveal a possible tendency of

 © 2017 Wiley-VCH Verlag GmbH & Co. KGaA, Weinheim

tryptophan towards the formation of well-organized fibrils with twisted structures.

In addition, the tryptophan amyloid fibrillary structures showed a clear cytotoxicity effect via triggering of well-regulated apoptotic cell death. Further examination should be applied, determining the different species of tryptophan structures, followed by their structural, biophysical, and biological analysis. Our new findings further extend the generic amyloid hypothesis to additional building blocks other than proteins and peptides and provide additional support to the association between several metabolic disorders and amyloid diseases.

5. Experimental Section

Materials

Tryptophan and alanine were purchased from Sigma (purity $\geq$98%). Fresh stock solutions were prepared by dissolving the amino acids at 90 °C in PBS or in Dulbecco's Modified Eagle Medium (DMEM):Nutrient Mixture F12 (Ham's) (1:1) (Biological Industries, Israel) at various concentrations ranging from 0.2 mg/mL to 4 mg/mL, followed by gradual cooling of the solution.

Transmission Electron Microscopy

Tryptophan was dissolved to 4 mg/mL at 90 °C in PBS, followed by gradual cooling of the solution. A 10 μL aliquot of this solution was placed on a 400 mesh copper grid. After 2 min, excess fluids were removed. Samples were viewed using a JEOL 1200EX electron microscope operating at 80 kV.

High-Resolution Scanning Electron Microscopy

Tryptophan was dissolved to 4 mg/mL at 90 °C in PBS, followed by gradual cooling of the solution. A 10 μL aliquot of this solution was placed on a glass slide and left to dry at room temperature. Samples were then coated with Cr and viewed using a JSM-6700 field-emission HR-SEM (Jeol, Tokyo, Japan), equipped with a cold field emission gun, operating at 10 kV.

Thioflavin T Staining and Confocal Laser Microscopy Imaging

Tryptophan was dissolved to 4 mg/mL at 90 °C in PBS, followed by gradual cooling of the solution. A 10 μL aliquot of ThT solution (2 mM in PBS) was mixed with 10 μL of the metabolite solution and placed on a glass microscope slide. The stained samples were visualized using an LSM 510 confocal laser scanning microscope (Carl Zeiss Jena, Germany) at excitation and emission wavelengths of 458 and 485 nm, respectively.

Thioflavin T Fluorescence Emission Spectra

Tryptophan was dissolved to 4 mg/mL at 90 °C in PBS, followed by gradual cooling of the solution. An aged sample of tryptophan was then added to 40 μM ThT in PBS to a final concentration of 20 μM ThT. With excitation set at 430 nm, the ThT fluorescence emission spectrum between 460 nm and 600 nm was collected via the Tecan Infinite M200 PRO Series fluorescent microplate reader.

Cell Cytotoxicity Experiments

The SH-SY5Y cell line (2×10^5 cells/mL) was cultured in 96-well tissue microplates (100 μL/well) and allowed to adhere overnight at 37 °C. Tryptophan and alanine were dissolved at 90 °C in DMEM:Nutrient Mixture F12 (Ham's) (1:1) (Biological Industries, Israel) at various concentrations ranging from 0.2 mg/mL to 4 mg/mL, followed by gradual cooling of the solution. Each plate was divided and only half of it was plated with cells. The negative control, represented by zero, was prepared as medium with no amino acids and treated in the same manner. 100 μL of medium with or without amino acids was added to each well. Following incubation for six hours at 37 °C, cell viability was evaluated using the 2,3-bis(2-methoxy-4-nitro-5-sulfophenyl)-2*H*-tetrazolium-5-carboxanilide (XTT) cell proliferation assay kit (Biological Industries, Israel) according to the manufacturer's instructions. Briefly, 100 μL of the activation reagent was added to 5 mL of the XTT reagent, followed by the addition of 100 μL of Activated-XTT Solution to each well. After 2.5 hours of incubation at 37 °C, color intensity was measured using an ELISA microplate reader at 450 nm and 630 nm. Results are presented as mean ± the standard error of the mean. Each experiment was repeated three times.

Flow Cytometry for Apoptosis Studies

Tryptophan and alanine were dissolved at 90 °C in DMEM:Nutrient Mixture F12 (Ham's) (1:1) (Biological Industries, Israel) at various concentrations ranging from 0.2 mg/mL to 4 mg/mL, followed by gradual cooling of the solution. SH-SY5Y cells were seeded at 2×10^5/well in six-well plates, and were allowed to adhere overnight at 37 °C, followed by incubation with medium containing metabolites for 24 h. Control cells were incubated with medium treated in the same manner without any addition of amino acids. The apoptotic effect was evaluated using the MEBCYTO Apoptosis Kit (MBL International, USA), according to the manufacturer's instructions. Briefly, the adherent cells were trypsinized, detached, and combined with floating cells from the original growth medium. They were then centrifuged and washed once with PBS and once with binding buffer. Cells were incu-

© 2017 Wiley-VCH Verlag GmbH & Co. KGaA, Weinheim

bated with annexin V–FITC and PI for 15 min in the dark, then resuspended in 400 μL of binding buffer and analyzed by flow cytometry using a single laser emitting excitation light at 488 nm. Data from at least 104 cells were acquired using BD FACSort and the CellQuest software (BD Biosciences, USA). Analyses were performed using the FlowJo software (TreeStar, Version 14). Each experiment was repeated three times.

Computational Methods

Two different tryptophan crystals[19] were modeled in all-atomistic simulations: (i) a small system of 288 molecules (12×12×2), which has only one layer of zwitterion aggregation in the crystal; and (ii) a large system of 1536 molecules (16×16×6), which has three layers of zwitterion aggregation. Both simulations were performed with the NAMD[20] package, using the CHARMM force field[22]. Fibrils were placed in an aqueous environment, with [NaCl] = 0.15 M to emulate cellular (physiological) conditions. The Langevin dynamics with a damping coefficient of 1 ps-1 and a time step of 1 fs was used to describe systems in a NPT ensemble at a pressure of 1 atm and a temperature of 310 K. During production run equilibration simulations particle mesh Ewald[21] was used with a grid spacing of 1.0. The SHAKE algorithm was used for the hydrogen atoms. Non-bonded interactions were evaluated at every time step, and full electrostatics were evaluated at every second time step. The non-bonded interactions used the switching algorithm, with the switch on distance at 10 Å and the switch off at 12 Å. Non-bonded pair lists were 13.5 Å, with the list updated every 20 steps. During minimization and pre-equilibration runs, all the heavy atoms of amino acids were subjected to large constraints so that dissolution would not occur. During equilibration runs, all heavy atoms in one molecule within each crystal were subjected to 20% of the previous constraints, whereas the remaining molecules were not subjected to constraints. The constraint on a single molecule was applied to prevent the crystal as a whole from leaving the primary box. Data and snapshots were recorded every 10 ps

Author Contributions

S.S.-N., L.A.-A., and E.G. conceived and designed the experiments. S.S.-N. planned and performed the experiments. P.R., L.V., and P.K. planned and performed the MD simulations. S.S.-N., L.A.-A., P.R., L.V., P.K., and E.G. wrote the paper. All authors discussed the results, provided intellectual input and critical feedback, and commented on the manuscript. Correspondence and requests for materials should be addressed to ehudg@post.tau.ac.il, Tel.: (+972) 3-640-9030.

Acknowledgements

This work was supported by the Israel Science Foundation (Grant No. 802/15; E.G.), The Strauss Institute (fellowship; S.S.-N), and the NSF Division of Materials Research (Grant No. 1309765; P.K.). We thank Dr. Alex Barbul for confocal microscopy analysis, Dr. Orit Sagi-Assif for the FACS analysis, Dr. Vered Holdengreber for help with TEM analysis, and the members of the Gazit, Adler-Abramovich, Vuković, and Král groups for the helpful discussions.

References

[1] a) T. P. J. Knowles, M. Vendruscolo, C. M. Dobson, *Nat. Rev. Mol. Cell Biol.* **2014**, *15*, 384–396; b) D. Eisenberg, M. Jucker, *Cell* **2012**, *148*, 1188–1203; c) A. Kapurniotu, *ChemBioChem* **2012**, *13*, 27–29; d) A. K. Buell, C. Galvagnion, R. Gaspar, E. Sparr, M. Vendruscolo, T. P. J. Knowles, S. Linse, C. M. Dobson, *Proc. Natl. Acad. Sci. U.S.A.* **2014**, *111*, 7671–7676; e) Y. Porat, S. Kolusheva, R. Jelinek, E. Gazit, *Biochemistry* **2003**, *42*, 10971–10977; f) A. K. Buell, A. Dhulesia, D. A. White, T. P. J. Knowles, C. M. Dobson, M. E. Welland, *Angew. Chem. Int. Ed.* **2012**, *51*, 5247–5251.

[2] a) R. N. Rambaran, L. C. Serpell, *Prion* **2008**, *2*, 112–117; b) T. D. Do, N. E. de Almeida, N. E. LaPointe, A. Chamas, S. C. Feinstein, M. T. Bowers, *Anal. Chem.* **2015**, *88*, 868–876; c) A. K. Buell, E. K. Esbjörner, P. J. Riss, D. A. White, F. I. Aigbirhio, G. Toth, M. E. Welland, C. M. Dobson, T. P. J. Knowles, *Phys. Chem. Chem. Phys.* **2011**, *13*, 20044–20052.

[3] E. Gazit, *FASEB J.* **2002**, *16*, 77–83.

[4] a) H. Inouye, D. Sharma, W. J. Goux, D. A. Kirschner, *Biophys. J.* **2006**, *90*, 1774–1789; b) T. P. Vinod, R. Jelinek, H. Rapaport, *Chem. Commun.* **2015**, *51*, 3154–3157; c) O. S. Makin, L. C. Serpell, *FEBS J.* **2005**, *272*, 5950–5961; d) E. Gazit, *Bioinformatics* **2002**, *18*, 880–883.

[5] a) M. Reches, E. Gazit, *Science* **2003**, *300*, 625–627; b) M. Reches, E. Gazit, *Nat. Nanotechnol.* **2006**, *1*, 195–200; c) L. Adler-Abramovich, D. Aronov, P. Beker, M. Yevnin, S. Stempler, L. Buzhansky, G. Rosenman, E. Gazit, *Nat. Nanotechnol.* **2009**, *4*, 849–854.

[6] a) N. Amdursky, M. Molotskii, D. Aronov, L. Adler-Abramovich, E. Gazit, G. Rosenman, *Nano Lett.* **2009**, *9*, 3111–3115; b) D. Pinotsi, A. K. Buell, C. M. Dobson, G. S. Kaminski-Schierle, C. F. Kaminski, *ChemBioChem* **2013**, *14*, 846–850; c) M. I. Souza, E. R. Silva, Y. M. Jaques, F. F. Ferreira, E. E. Fileti, W. A. Alves, *J. Pept. Sci.* **2014**, *20*, 554–562.

[7] a) S. Grudzielanek, A. Velkova, A. Shukla, V. Smirnovas, M. Tatarek-Nossol, H. Rehage, A. Kapurniotu, R. Winter, *J. Mol. Biol.* **2007**, *370*, 372–384; b) D. T. Loo, A. Copani, C. J. Pike, E. R. Whittemore, A. J. Walencewicz, C. W. Cotman, *Proc. Natl. Acad. Sci. U.S.A.* **1993**, *90*, 7951–7955; c) F. M. LaFerla, B. T. Tinkle, C. J. Bieberich, C. C. Haudenschild, G. Jay, *Nat. Genet.* **1995**, *9*, 21–30; d) Y. P. Li, A. F. Bushnell, C. M. Lee, L. S. Perlmutter, S. K. F. Wong, *Brain Res.* **1996**, *738*, 196–204; e) Y. Bram, A. Frydman-Marom, I. Yanai, S. Gilead, R. Shaltiel-Karyo, N. Amdursky, E. Gazit, *Sci. Rep.* **2014**, *4*, 426.

[8] a) L. Adler-Abramovich, L. Vaks, O. Carny, D. Trudler, A. Magno, A. Caflisch, D. Frenkel, E. Gazit, *Nat. Chem. Biol.*

© 2017 Wiley-VCH Verlag GmbH & Co. KGaA, Weinheim

2012, *8*, 701–706; b) A. S. Rosa, A. C. Cutro, M. A. Frías, E. A. Disalvo, *J. Phys. Chem. B* **2015**, *119*, 15844–15847; c) T. D. Do, W. M. Kincannon, M. T. Bowers, *J. Am. Chem. Soc.* **2015**, *137*, 10080–10083.

[9] D. Ferrier, R. Harvey, *Lippincott's Illustrated Reviews: Biochemistry*, Lippincott Williams & Wilkins, Philadelphia, USA, **2014**.

[10] S. Shaham-Niv, L. Adler-Abramovich, L. Schnaider, E. Gazit, *Sci. Adv.* **2015**, *1*, e1500137

[11] A. P. Pawar, K. F. DuBay, J. Zurdo, F. Chiti, M. Vendruscolo, C. M. Dobson, *J. Mol. Biol.* **2005**, *350*, 379–392.

[12] P. W. Frederix, G. G. Scott, Y. M. Abul-Haija, D. Kalafatovic, C. G. Pappas, N. Javid, T. H. Neil, R. V. Ulijn, T. Tuttle, *Nat. Chem.* **2015**, *7*, 30–37.

[13] C. M. Santiveri, M. Jiménez, *Pept. Sci.* **2010**, *94*, 779–790.

[14] D. M. Richard, M. A. Dawes, C. W. Mathias, A. Acheson, N. Hill-Kapturczak, D. M. Dougherty, *Int. J. Tryptophan Res.* **2009**, *2*, 45–60.

[15] a) J. R. Martin, C. S. Mellor, F. C. Fraser, *Clin. Genet.* **1995**, *47*, 180–183; b) "Hypertryptophanemia", Orphanet, June **2006**, as accessed on the website: http://www.orpha.net/consor/cgi-bin/OC_Exp.php?Lng=GB&Expert=2224; c) "Hypertryptophanemia, Familial" (OMIM: 600627), September **2014**, as accessed on the website: http://www.omim.org/entry/600627.

[16] "Hartnup Disorder; HND" (OMIM: 234500), July **2014**, as accessed on the website: https://omim.org/entry/234500.

[17] *The Online Metabolic and Molecular Bases of Inherited Disease* (Eds.: D. Valle, A. L. Beudet, B. Vogelstein, K. W. Kinzler, S. E. Antonarakis, A. Ballabio, K. M. Gibson, G. Mitchell), McGraw-Hill, New York, **2014**.

[18] L. Milanesi, W. Xue, T. Sheynis, E. V. Orlova, A. L. Hellewell, R. Jelinek, E. W. Hewitt, S. E. Radford, H. R. Saibil, *Proc. Natl. Acad. Sci. USA.* **2012**, *109*, 20455–20460.

[19] C. H. Görbitz, K. W. Törnroos, G. M. Day, *Acta Crystallogr., Sect. B: Struct. Sci.* **2012**, *68*, 549–557.

[20] J. C. Phillips, R. Braun, W. Wang, J. Gumbart, E. Tajkhorshid, E. Villa, C. Chipot, R. D. Skeel, L. Kalé, K. Schulten, *J. Comput. Chem.* **2005**, *26*, 1781–1802.

[21] T. Darden, D. York, L. Pedersen, *J. Chem. Phys.* **1993**, *98*, 10089–10092.

[22] a) K. Vanommeslaeghe, E. Hatcher, C. Acharya, S. Kundu, S. Zhong, J. Shim, E. Darian, O. Guvench, P. Lopes, I. Vorobyov, A. D. Mackerell Jr., *J. Comput. Chem.* **2010**, *31*, 671–690; b) K. Vanommeslaeghe, A. D. MacKerell Jr., *J. Chem. Inf. Model.* **2012**, *52*, 3144–3154; c) K. Vanommeslaeghe, E. P. Raman, A. D. MacKerell Jr., *J. Chem. Inf. Model.* **2012**, *52*, 3155–3168; d) A. D. MacKerell Jr., D. Bashford, M. Bellott, R. L. Dunbrack Jr., J. D. Evanseck, M. J. Field, S. Fischer, J. Gao, H. Guo, S. Ha, D. Joseph-McCarthy, L. Kuchnir, K. Kuczera, F. T. K. Lau, C. Mattos, S. Michnick, T. Ngo, D. T. Nguyen, B. Prodhom, W. E. Reiher, B. Roux, M. Schlenkrich, J. C. Smith, R. Stote, J. Straub, M. Watanabe, J. Wiórkiewicz-Kuczera, D. Yin, M. Karplus, *J. Phys. Chem. B* **1998**, *102*, 3586–3616; e) A. D. Mackerell Jr., M. Feig, C. L. Brooks, *J. Comput. Chem.* **2004**, *25*, 1400–1415.

[23] E. Mossou, S. C. M. Teixeira, E. P. Mitchell, S. A. Mason, L. Adler-Abramovich, E. Gazit, V. T. Forsyth, *Acta Crystallogr., Sect. C* **2014**, *C70*, 326–331.

[24] C. H. Görbitz, *Chem. Commun.* **2006**, 2332–2334.

Received: June 29, 2016
Published online: November 16, 2016

© 2017 Wiley-VCH Verlag GmbH & Co. KGaA, Weinheim